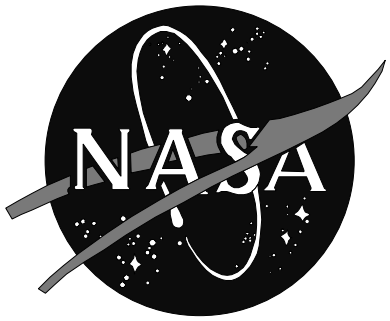


# COMPARISON OF INTEGRATED ANALYSIS METHODS FOR TWO MODEL SCENARIOS

**Ninth Thermal and Fluids Analysis Workshop**
August 31 - September 4, 1998
Cleveland, Ohio

**Ruth M. Amundsen**
National Aeronautics and Space Administration
Langley Research Center
Hampton VA 23681-2199

# COMPARISON OF INTEGRATED ANALYSIS METHODS FOR TWO MODEL SCENARIOS

Ruth M. Amundsen
National Aeronautics and Space Administration
Langley Research Center
Hampton VA 23681-2199

## SUMMARY

Integrated analysis methods have the potential to substantially decrease the time required for analysis modeling. Integration with computer aided design (CAD) software can also allow a model to be more accurate by facilitating import of exact design geometry. However, the integrated method utilized must sometimes be tailored to the specific modeling situation, in order to make the process most efficient. Two cases are presented here that illustrate different processes used for thermal analysis on two different models. These examples are used to illustrate how the requirements, available input, expected output, and tools available all affect the process selected by the analyst for the most efficient and effective analysis.

## INTRODUCTION

Integrated analysis methods can substantially reduce the time and effort required to produce analytical results, and also potentially offer improved accuracy. By importing model geometry electronically, time spent in manual creation of geometry is eliminated, and the model created reflects the exact design. By sharing a model between the structural and thermal analysts, the time to develop a model can be cut in half. This also ensures that the analysts are working with the same version of the geometry. The direct access between thermal and structural models facilitates solution for problems that are driven by thermally induced stress. The exact methods and tools used in integrated analysis can vary depending on the type of analysis, the model geometry, and the expected variation in cases to be run. Shown here are two examples of integrated modeling approaches that differ based on the modeling requirements.

The first case discussed is the thermal analysis of a hypersonic wing. In this situation, there were several different proposed geometries to be analyzed, which meant that efficient import from the CAD software was important. The heating loads were provided from an independent aeroheating code. These loads went through several iterations and parametric studies, so that efficient import of those values significantly reduced the total analysis time. The grid used for the aeroheating calculation was much coarser than the grid used for the thermal analysis; therefore, the heat load distribution required interpolation to the thermal analysis mesh. The aeroheating parameters were interpolated in time from the aeroheating calculation time steps to the much finer solution time steps used in MSC/PATRAN THERMAL (ref. 1). The method was tailored in that the calculated aeroheating rates were used only on the wing flat sections, and stagnation point heating was calculated separately and applied to the swept leading edge only. Radiation analysis within the wing was performed using the VIEWFACTOR module internal to PATRAN. Radiative loss to the atmosphere was also included. The predicted temperature distribution was required for structural MSC/NASTRAN (ref. 2) runs to determine if the wing temperature gradient produced excessive stresses.

The second case is that of a large space-based antenna array. The array consisted of multiple composite antenna waveguides, each six meters in length with a small open rectangular cross-section, supported by a truss structure of tubular composite struts and metal joints. In this case, the geometry was such that direct import from the CAD software was neither effective nor efficient. The model was built manually, using selected import of parts from the CAD software. The large size of the model drove the use of beams for truss members in order to simplify the model. Orbital fluxes and radiation conductors were calculated using the TRASYS (ref. 3) solver. Because of

limitations with beam elements in both PATRAN and TRASYS, a separate TRASYS model was required, using cylindrical surfaces for the truss members to calculate correct orbital flux loads. The transient heat loads from TRASYS were applied to the PATRAN model using fields, with liberal use of text file import and automated session files to minimize modeling time. The limitations of the current PATRAN version (7.5) with respect to beam elements required the use of interesting workarounds to apply radiation and heating boundary conditions to the truss. In this situation, there were several parametric runs performed within TRASYS, so the heat load application method was selected to provide simple substitution of TRASYS result cases. The temperature distributions were again required for NASTRAN structural runs, this time to determine thermally induced deflections of the array. The driving requirement on the array was to maintain stability within certain deflection tolerances; thermal cases were applied as loads using both the differences around a single orbit as well as differences over a year.

The tools used in each of these two cases were tailored to the needs of that situation, and modifications to the methods were made as necessary. Customizing the integrated analysis methods on the fly optimized the speed and accuracy of the analysis performed in each case.

## WING MODEL

### Requirements

Requirements on the hypersonic wing modeling approach were as follows. The analysis was to be performed on the horizontal wing of a hypersonic vehicle that was under design by a contractor. Several geometry configurations and material combinations had been proposed and required analysis. Thus, it was important that the modeling approach simplify analyzing changes to the geometry and materials. The main thermal loads on the wing were aerodynamic heating loads from the hypersonic airflow, predicted by an independent aeroheating code. There were several different criteria used to predict aeroheating, and improvements in the design trajectory were continually being made, which resulted in a large number of different aerodynamic load cases to be evaluated. Thus, it was crucial that the model be able to rapidly evaluate updates to the aeroheating loads. The mesh used in the aeroheating model was much coarser than the thermal model would need. Also, the aeroheating loads were only put out at 18 time steps along the 127-second trajectory, which was a much larger time step than would be used in the thermal analysis. Thus, it was critical that the thermal analysis provide accurate interpolation of the heating data (both in space and time) onto the thermal model. A different method was required to calculate and apply the stagnation point heating at the leading edge, without compromising the heat values applied from the aeroheating code. The wing body contained internal open cavities. The radiation within these was a significant factor in equalizing the thermal distribution across the wing. Radiation from the wing surface to the atmosphere was also required to be included. The atmospheric temperature was a variable since the altitude change over the time period in question was substantial. The selected modeling method needed to include radiation within the geometry, as well as to an external variable temperature. Finally, the temperature prediction output was needed not only to determine if all materials would survive, but also for structural analysis. The temperature gradient was the main driver in creating stresses on the wing. Thus, a simple method for translating the thermal gradient to a structural model load was necessary.

### Geometry Modeling

These requirements were satisfied by the methodology chosen, which included using MSC/PATRAN to model the wing. The geometry was imported electronically from the computer-aided design (CAD) software Pro/Engineer (ref. 4). After the geometry was imported into PATRAN, it existed as “trimmed solid” geometry. Using the current version of PATRAN (v. 7.5), it was only possible to mesh this with a tetrahedral mesh. For the structural model this was acceptable. For the thermal model, however, a more detailed hex mesh was desired near the leading edge where the extremely high heat loads and high gradients occurred. In the baseline design, the wing consisted of two parts, as shown in Figure 1. A tetrahedral mesh was acceptable on the aft or body portion of the

wing. For the leading edge portion, native PATRAN ("blue") solids were created from the imported trimmed solid, thus allowing an automated brick or hex mesh. Boundary conditions such as convection and radiation were applied only to the geometry faces. This allowed several different meshing densities to be evaluated without reapplying boundary conditions. When a new geometry was to be evaluated, a copy of the entire database was used that included material properties, boundary conditions, analysis parameters, boundary nodes and all fields. The original geometry and mesh were deleted, and the new geometry imported. Boundary conditions and properties then only needed to be modified rather than recreated. When a new geometry was brought in, it was possible to have the new model meshed and running in less than four hours. Most of the model sizes were in the range of 10000 to 30000 nodes. To compare geometries' performance, it was sometimes possible to use the trimmed solid geometry and a solely tetrahedral mesh. This did not allow the true curve of the leading edge to be represented. However, it was found that the difference in area between the curved leading edge and the flat edge presented by the tetrahedral mesh could be applied as a factor on the stagnation point heating. This was useful for qualitative comparisons of geometries; the thermal error it induced was determined to be less than 5%.

## Boundary Conditions

The boundary conditions used were radiation within the cavities, radiation from the wing exterior, contact conductance, aeroheating convection to the top and bottom surfaces of the wing and stagnation point heating at the wing leading edge. Although temperature-dependent emissivity was an option, it was not used in this case since the emissivities were fairly constant with temperature, and the additional accuracy was not felt to be worth the sacrifice in solution speed. The internal PATRAN module VIEWFACTOR handled the radiation within the cavities. The viewfactors were run with several different tolerances and zero factors. Once the viewfactors had been run for a particular geometry, they could be re-used for subsequent runs of that geometry without recalculation. The radiation from the exterior surface of the wing to the atmosphere was done using the "between regions" radiation boundary condition. A boundary node for the atmosphere was created. The model was run initially with a constant temperature for the atmosphere; later this was revised to a variable temperature boundary condition to reflect the change in temperature with altitude.

## Aeroheating Loads

FORTRAN subroutines were developed to perform the interpolation of aeroheating loads to the PATRAN model. The aeroheating model included all wing variables that changed as a function of time, such as wing angle of attack (AOA), altitude, mach number, etc. There are many routines built into PATRAN that allow the user to modify operation of the PATRAN THERMAL solver; four of these were utilized in this case. The first is a uinit.f routine, which is called once to initialize parameters before solution of the problem. Modification of this file allows the user to initialize files for later output. In this case, a file named uopen_trans.f was called within uinit.f. This file read in the aeroheating files and loaded them into arrays. Within the uopen_trans routine, the loads file values and co-ordinates were translated into the units and axes used in the PATRAN model. This is a valuable feature of this process – the units and coordinates in the loads file can differ from those used in the PATRAN model without interfering with the smooth transfer of data. A required uncertainty factor that was variable with time was applied to the values before loading them into the array. The next file, normally called by PATRAN at every solution iteration, is uhval.f. This file is activated by having a convective boundary condition ID greater than 1000 applied, and allows the user to define the desired convection configuration. The spatial interpolation requires only 2D interpolation since the location of any point on either the top or bottom surface of the wing is completely defined by the x and y location.

The interpolation of the loads incorporated some interesting features. The leading edge of the wing, where the highest gradients of heating and temperatures occurred, is highly swept (65° from normal). An example of the interpolated $h_c$ (convective coefficient) values and their high gradients near the leading edge is shown in Figure 2. The aeroheating mesh was relatively coarse. Near the leading edge, both the aeroheating mesh and the PATRAN mesh followed the sweep angle of the leading edge. Due to the coarseness of the aeroheating mesh, the aeroheating grid spatially closest to a given PATRAN node was not always the best one to use for interpolation,

since it might be at a location substantially further from the leading edge. Thus, a method had to be developed to handle the interpolation correctly and weight the values using the distance from the leading edge.

The interpolation in time from the 18 time steps of the trajectory to the solution time steps used in PATRAN THERMAL was necessary since the average aeroheating time step was about 10 seconds, and the average PATRAN solution time step was about 0.1 seconds. The values used within PATRAN THERMAL were interpolated in a weighted fashion from the two closest points in time from the trajectory, with the heating at time zero assumed to be zero.

Another aspect of the aeroheating model that required modification was the leading edge heat flux. The $h_c$ values over the curved leading edge portion had to be calculated outside of the aeroheating code. The stagnation point $h_c$ values were calculated separately using FORTRAN software that used Fay-Riddell methods. These values were calculated over the same 18-point trajectory. The stagnation point values were placed in a mat.dat.apnd file and applied as a separate boundary condition. The node points on the tangent (between the curve of the leading edge and the flat wing section) received a combination of heating values. The leading edge curve elements had the stagnation point $h_c$ applied, and the flat section elements had the aeroheating load file values applied. Nodes that joined these two elements received the stagnation point heat flux on the area associated with the element on the curved face, and the load file heat flux on the area associated with the flat section element. Thus the total heat applied to these nodes was an average correctly weighted by area.

## Radiation

The radiation within the wing cavities was calculated by the internal PATRAN module VIEWFACTOR. Several runs were made with different zero tolerance values on the grey body factors. The optimum tolerance value was determined by taking the value at which there were no substantial changes in viewfactors due to a decrease in the tolerance. These calculated radiation conductors were then used in subsequent runs without the necessity for re-calculation.

Radiation from the wing exterior to the atmosphere is an important factor in controlling the wing temperature rise. The two materials on the exterior had relatively flat emissivity curves (little change in emissivity with temperature over the expected temperature range), so a constant emissivity was assumed. The radiation “between regions” boundary condition was used, with a radiation boundary node as the sink. The temperature of this node was originally approximated as a fixed temperature, and was later improved to reflect the change in atmospheric temperature with altitude over the trajectory. This small increase in model accuracy made very little difference in the model results.

## Contact Conductance

Since several of the wing geometries evaluated consisted of two or more separate parts, and since there were high temperature differences between parts, the contact conductance between them was an important variable. The parts were in general attached via pinned connections, with little or no contact pressure. The gap between the parts would be dependent on machining tolerances, and would vary with temperature. No data on contact conductance between the candidate material types was found. For these reasons, the contact conductance problem was bounded by using minimum and maximum reasonable values to determine the worst-case. The minimum value was calculated by assuming no contact, with heat transfer via radiation and conduction through still air across the maximum gap distance. The maximum contact conductance value was determined by utilizing the maximum no-contact-pressure value found for dissimilar materials in the published data. Contact conductance between parts was simple to apply in PATRAN. After the parts were meshed, they were equivalanced individually, so that nodes on the boundary between the parts were not equivalanced together. The convection “between regions” boundary condition was used to simulate contact. This boundary condition was applied to the geometry, so that re-meshing operations would not force extensive model modification.

### Results

The temperature output of the model was used for two purposes. First, the temperatures of each component in each geometry case were compared to the single-use temperature limits for that material. This allowed a determination of which design configurations would allow the materials to survive thermally. An example plot of the thermal distribution is shown in Figure 3. The gradients at the leading edge, apex and around the geometry pockets in the aft wing body are evident from the plot; these complex three-dimensional gradients are the main reason that this fully representational geometry model is necessary. This type of plot allowed the user to determine specifically what portions of each part were exceeding thermal limits, and at what solution times this was occurring. The thermal results are highly time-dependent, as shown in the example thermal transient chart (Figure 4). This illustrates why all time-varying features of the problem must be considered, such as Mach number, altitude, wing angle of attack, etc. The second use for the temperatures was translation to the structural model, which in some cases had a different mesh, to allow a structural analysis of the wing that combined thermal stresses and stresses induced by the air pressure loading. The temperature gradients on each design were the main drivers in producing large deflections and stresses. The deflections and stresses predicted for each design were the major factors utilized in selecting a final vehicle configuration. The use of a fully three-dimensional thermal gradient to predict the actual stress condition of the wing was found to be much more accurate than using two-dimensional cuts of the wing to approximate the thermal distribution.

## ORBITING ANTENNA ARRAY MODEL

### Requirements

The second modeling scenario is that of a large orbiting space-based antenna array. The modeling approach for this system had very different constraints than the hypersonic wing. Instead of being a single part with relatively small-scale geometry, the antenna array was a complex assembly with a large spatial extent, as shown in Figure 5. However, there was only one proposed geometry to be evaluated, so that variation of the assembly geometry was not a driving factor in the modeling approach. One factor in the geometry that was known in advance to be variable was the support strut diameter, so it was desirable to select a method that simplified this alteration. Several materials and several orbit conditions were to be evaluated, so facilitating the change of boundary conditions was important. Since this was an orbiting space-based array, correct radiation conductors and orbital fluxes for the surfaces were critical. Schedule constraints were an incentive to build a common model utilized by both the structural and thermal analysts. The main science requirement on the array was to minimize the on-orbit deflection of the waveguides with respect to each other. These deflections were mainly driven by the thermal gradients, since the array was orbiting in 0-g, and outside of atmospheric drag. Thus, similar to the wing model, an important factor in selecting the methodology was efficient transfer of temperatures to the structural analysis model.

### Geometry Modeling Method

The constraints were efficiently met using a combined analysis methodology that utilized both PATRAN and TRASYS, as well as some “manual” model development. The array was composed of 16 waveguides, each 6 m in length with an open rectangular cross-section of 14.5 x 7 cm. This gave an inherent length ratio in the geometry of the thinnest face of 86:1. The waveguides were connected via a truss of tubular struts. The strut lengths varied from 0.1 to 1 meter, with a diameter of 2.5 cm, for a maximum length-to-diameter ratio of 40:1. The joints where struts were connected were extremely complex, involving a transition from composite truss to metallic joint, as well as rotational and locking capability within the joint. There were several dozen separate parts within each joint, and over 100 joints in the entire assembly. When this entire assembly was pulled in electronically from the CAD software Pro/Engineer, it created an extremely large PATRAN database, even prior to meshing. An entirely electronic imported geometry model would not have been reasonable in this case. The

model would have been too large to allow solution in a reasonable time, would not have allowed simple change of materials or orbital conditions, and would not have allowed simple application of rotational boundary conditions on the revolute joints. In addition, since the strut tubes were imported as trimmed solids, these extremely thin-walled struts would have been meshed with a tetrahedral solid mesh, which would not have been efficient or accurate. The diameters of the strut tubes could not have been modified in a simple way. In order to overcome these limitations, it was decided to build the model using PATRAN native shapes (plates and beams) with dimensions and positions from the Pro/Engineer geometry. The Pro/Engineer model was used to create an IGES file of the assembly parts' shapes and positions. This IGES file was imported into PATRAN and used to expedite geometry definition. The model was constructed using plates for the waveguide sides and beams for the struts. This gave the simplest model and facilitated the connection and application of boundary conditions in both the thermal and structural analysis. It also permitted simple force recovery in the struts. The joints were modeled as beams of the metallic material, with the correct cross-sectional area and length. This allowed the correct prediction of thermally-driven expansion and distortion, but simplified the modeling of joint connections. Since it had been determined that only a single geometry configuration would be evaluated, the time spent in manual model development was not as detrimental as it would have been for a system with continually changing geometry such as the wing.

Since the model geometry was developed manually, parts could be grouped as necessary so that alternate materials for struts, joints and waveguides could be easily analyzed. An additional benefit of using beams for the struts was that diameters different than the baseline design could be evaluated without re-meshing or re-applying boundary conditions. The model that was constructed only contained half the array (eight waveguides), since the two halves were relatively similar geometrically. The PATRAN model is shown in Figure 6. The meshed model contained roughly 13000 nodes.

## Orbital Fluxes and Radiation

The most challenging part of the modeling for the thermal analyst was the application of orbital flux boundary conditions. The VIEWFACTOR module would not handle orbital flux calculations. A translator from PATRAN to the TRASYS radiation and orbital flux software existed, but included several severe limitations. None of the beams would be translated, and the rectangular plates would be translated as the "POLY" surface type. At first, this problem would seem to be tailor-made for application of the Thermal Synthesizer System (TSS), since that would allow simple calculation of the orbital flux heating loads. There were two reasons this software was not used. First, because of hardware limitations, there was not a running copy of TSS at NASA Langley at the time. Second, since the structural analysis would be performed from a PATRAN model, and the thermal analyst was to build that model, it saved a substantial amount of time to perform the thermal analysis using the same PATRAN model. The most efficient solution found was to re-build the geometry in TRASYS. The TRASYS model is shown in Figure 5. This allowed calculation of the transient orbital fluxes to each surface. Since the geometry was extremely sparse, most of the viewfactors of elements to space were unity. Viewfactors were calculated within TRASYS, but in most cases were averaged or rounded to unity when applying the radiation conductors within PATRAN. Only four distinct regions of different radiation-to-space factors were used in the PATRAN model, and these were applied via the "between regions" radiation boundary condition (which does not call the VIEWFACTOR module).

Much of the geometry information could be exported from the PATRAN model and used to place and size elements of the TRASYS model. However, there were several challenges inherent in the re-build of the geometry. First, in the TRASYS version used (version 2.7) the bar "ELEM" element type analogous to the PATRAN beam is not fully functional and does not provide accurate results. Thus, the strut and joint beams required construction as cylinders. Since they had fairly large length-to-diameter ratios, most of them were multiply noded, with the results averaged via correspondence data. Each surface area had a boundary condition applied for orbital flux, as well as a boundary condition for radiation to space. A completely integrated method for applying radiation-to-space to the PATRAN beam elements did not exist. Up through version 7.5 of PATRAN there is no way to convect or radiate from 1D conduction bars in 3D space. The workaround was to apply a boundary condition to the beams that was a variable nodal heat source on the bar nodes. The boundary condition template ID defined

the space node as the ambient node and called a straight-line microfunction that defined the heat as a workaround for radiation out. For radiation the independent variable was "Radiosity Difference," $\sigma*(T_1^4 - T_{amb}^4)$, where $\sigma$ is the Stefan-Boltzmann constant, $T_1$ is the nodal temperature, and $T_{amb}$ is the ambient radiation sink temperature. P1, the slope, was $-\varepsilon*A/2$, where $\varepsilon$ was the emissivity of the bar and A was the total perimeter area of the bar (the negative was necessary to have the correct direction on heat flow). The value of P2, the intercept, was 0.0. A new microfunction was required for every beam element with a different area (ref. 5).

There were 460 regions in the TRASYS model that had different orbital heat flux transients to be applied to the PATRAN model, as well as 16 types of beams with different areas that required the radiation workaround heating boundary condition. There were two orbit extremes to be evaluated (solar $\beta = 90°$ and solar $\beta = 60°$). There were two halves of the array to be evaluated, one of which was extensively shaded by the spacecraft, and the other receiving direct sun in the $\beta=90°$ orbit. At first, the application of 460 boundary conditions for four different transient orbital conditions would seem an overwhelming task. However, the orbital flux values produced by TRASYS were in a text file, formatted in arrays of heat flux versus time. These could be manipulated in Microsoft Excel so that the format matched that required by PATRAN THERMAL in the micro.dat.apnd file. PATRAN THERMAL uses this file during execution to define time- and temperature-varying fields. The macros (command sequences) in Excel for performing this manipulation were saved so that they could be used on subsequent data sets. For the $\beta=60°$ orbit, there were 48 time steps in each orbit, and eight consecutive orbits were run to achieve stable repeating results. Using the micro.dat.apnd file, all of the fields could be constructed and applied via external text files. The template.dat.apnd file relating the boundary condition template ID to the appropriate microfunction was also simply generated in Excel. Most of the boundary conditions were applied to the PATRAN model in a repetitive manner, using editing of session files. Once a boundary condition had been applied to one portion of the model, that session file could be duplicated and edited to allow more automated application of boundary conditions. This substantially reduced the time required to apply all the boundary conditions. Evaluation of a different orbit condition was relatively simple -- none of the boundary conditions needed to be changed. The only alteration was to construct a new micro.dat.apnd file from the TRASYS output file, and use that file in the thermal analysis run. This facilitated switching between the two halves of the array, as well as evaluation of other orbital parameters and material properties. Once an analysis had been developed in this manner, alteration to evaluate another orbital condition could be done in less than an hour.

Another consideration in this model was the conflict between boundary conditions (BCs). Each of the beam elements had two heat source boundary conditions applied: the actual orbital heating, and the radiation workaround. If these were run in the same thermal load case, there was a choice between adding the conditions together, or setting an overwrite priority. Obviously, neither the radiation nor orbital heating should be overwritten. However, if "Add" was selected under the load case definition, then nodes at the intersection of two different beam heating BC's received double the correct amount of heating, because the beam heating BC did not weight heating by element area. The solution implemented for this problem was to use "Overwrite" in the load case definition, so that intersection nodes received the correct heating. Then two different load cases were run to create two different qmacro.dat files, one for radiation psuedo-heating, and one for true orbital heating. These qmacro.dat files were then manually combined and the full model was run using the combined qmacro file.

## Results

The temperatures output from this analysis were quite easy to import into the structural model (in PATRAN, execute File…Import…Results), since the same mesh was used. Nodes used in thermal analysis but not in structural (such as the ambient space node) did not affect this transfer. The model was run for two array halves (one extensively shaded by the spacecraft, one with more direct solar flux) and for two different orbit conditions ($\beta=60°$ and $\beta=90°$). Each of these four conditions was evaluated for structural predictions. The predicted behavior of the array on initial entry into orbit (using several different assumptions for launch time), as well as the orbital and annual transients, were all determined in both the thermal and structural analyses. An example thermal distribution is shown in Figure 7. The predicted thermal distributions were also used to ensure that no material or component went outside its operational temperature range. Transient plots for each run were

constructed for selected nodes, using session files and the applicable routine in the patq executable. This enabled simple determination of whether the model had been run for a sufficient number of orbits to achieve stability. An animation of the transient distribution as a changing color map on the PATRAN model was constructed and transferred to video to enhance visualization of the thermal behavior. The animation was also placed on a Web page.

## CONCLUSIONS

Unique integrated thermal analysis techniques using PATRAN, PATRAN THERMAL, TRASYS, and import from Pro/Engineer were applied to resolve potential thermal problems for an advanced hypersonic wing shape and a large orbiting antenna array. In each of these cases, the modeling approach was tailored to suit the modeling requirements and constraints. In the hypersonic wing case, the important parameters were to expedite alteration of geometry and materials, incorporate complex transient aeroheating gradients, and translate temperature distributions to the structural analysis. Extensive use of electronic import from Pro/Engineer into PATRAN, editing of PATRAN THERMAL subroutines, VIEWFACTOR radiation calculation, and boundary conditions applied to geometric entities were found to comprise the most efficient thermal analysis method for this case. In the orbiting array case, the critical factors were to provide a usable structural model, apply orbital heating, facilitate changes to certain geometry parameters, and translate temperature distributions to the structural analysis. This scenario required manual model development to minimize model size and increase usability, extensive text and session file use for boundary condition application, and novel workarounds for beam heating and radiation. Both cases effectively used integrated methods to decrease the time required for analysis and increase the accuracy of the final predictions.

## ACKNOWLEDGEMENTS

The assistance of the structural analyst, Michael Lindell, in developing PATRAN models and providing modeling advice is gratefully acknowledged. The re-use of FORTRAN software developed and modified by Phil Yarrington is acknowledged with thanks. The assistance of Abel Torres and Chuck Leonard in providing aeroheating data and assistance is deeply appreciated.

## ACRONYMS

| | |
|---|---|
| AOA | Angle of Attack |
| BC | Boundary Condition |
| CAD | Computer Aided Design |
| CFD | Computational Fluid Dynamics |
| FEM | Finite Element Model |
| ID | Identification Number |
| IGES | Initial Graphics Exchange Specification |
| TSS | Thermal Synthesizer System |

## SYMBOLS

| | |
|---|---|
| $A$ | Area |
| $\varepsilon$ | Emissivity |
| $h_c$ | Convective Heat Transfer Coefficient |
| $\sigma$ | Stefan-Boltzmann Constant |
| $T_{amb}$ | Ambient Temperature |

REFERENCES


1. MSC/PATRAN User Manual, MacNeal-Schwendler Corporation, Version 7.5 (August 1996).
2. Kilroy, K., MSC/NASTRAN, Quick Reference Guide, The MacNeal-Schwendler Corporation, June 1997.
3. Thermal Radiation Analyzer System (TRASYS) User's Manual, JSC-22964, April 1988.
4. Parametric Technology Corporation, Pro/Mechanica Reference Manual, 1997.
5. PATRAN Technical Note 3251, http://www.macsch.com/


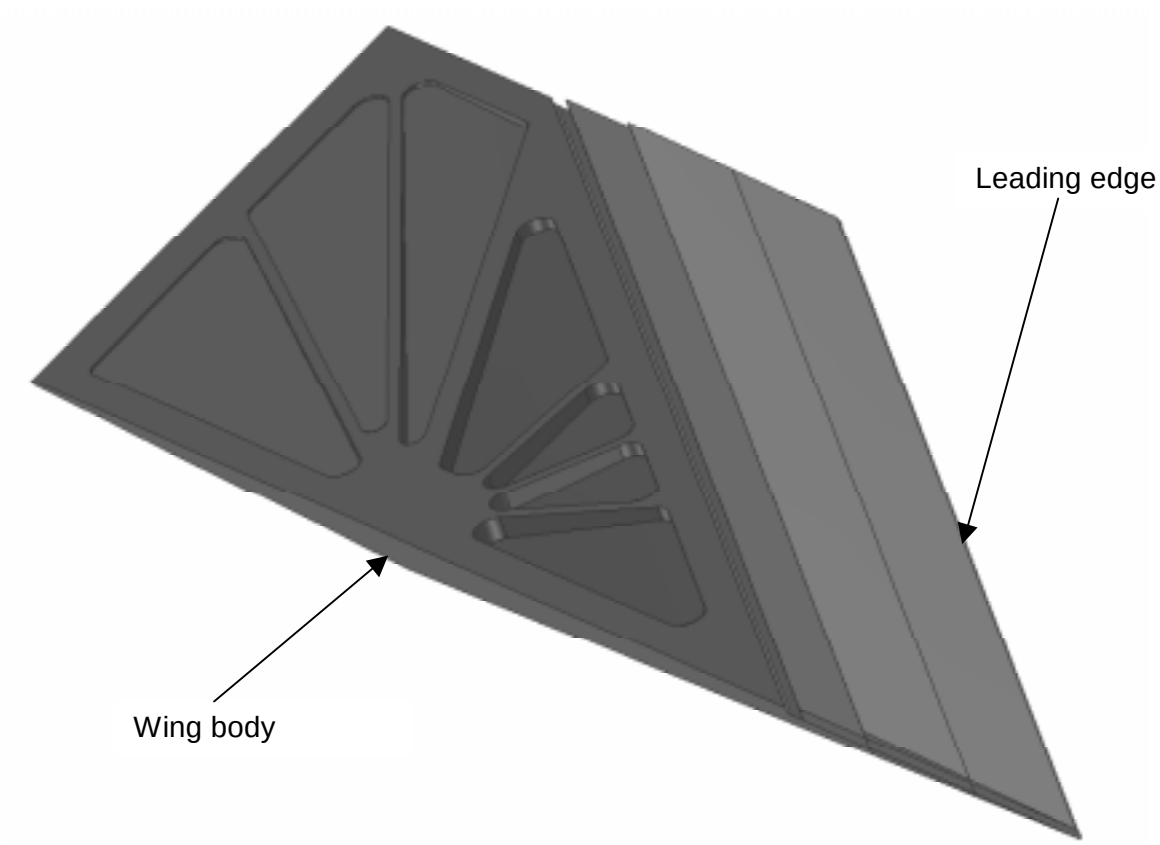


Figure 1. Hypersonic wing geometry (interior of wing body shown for illustration).

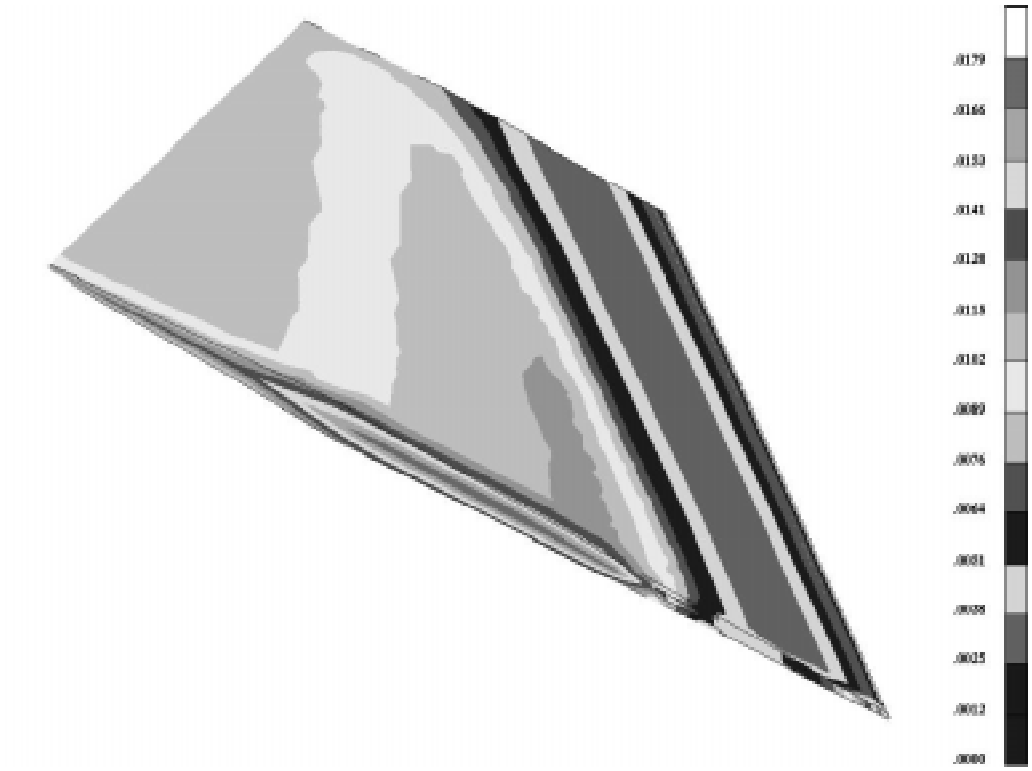


Figure 2. Example distribution of $h_r$ values over wing at one time point (arbitrary units).

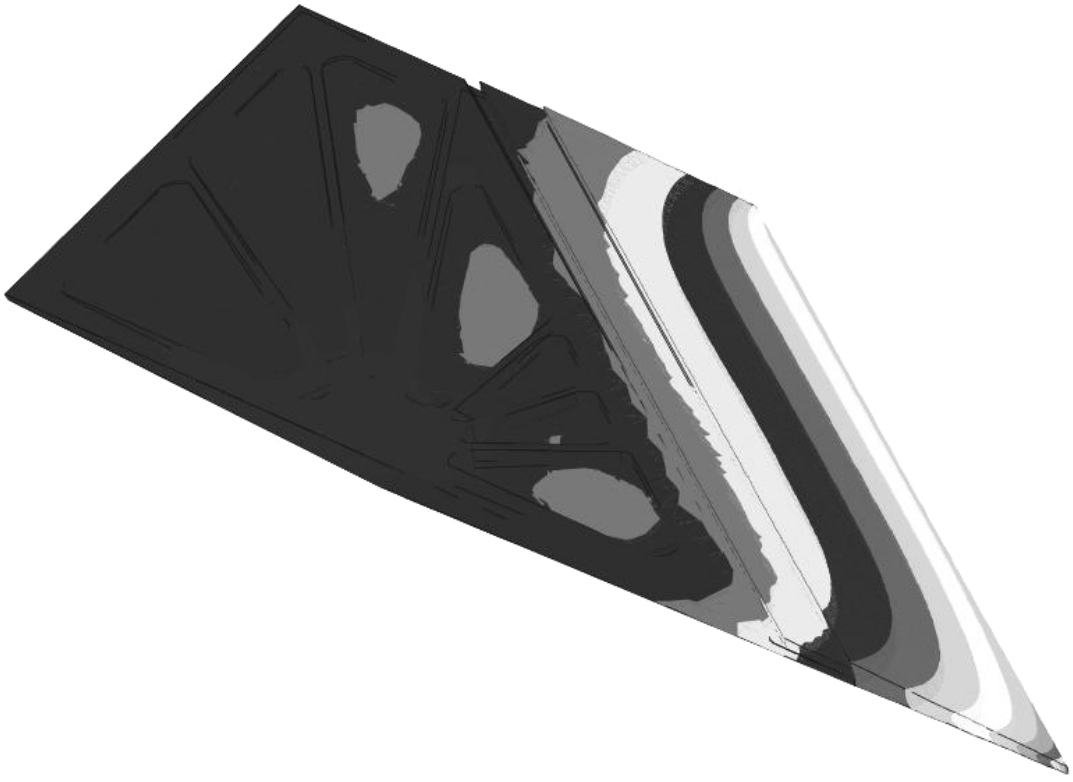

Figure 3. Example thermal distribution on hypersonic wing
(temperature values not disclosed due to information protection concerns).

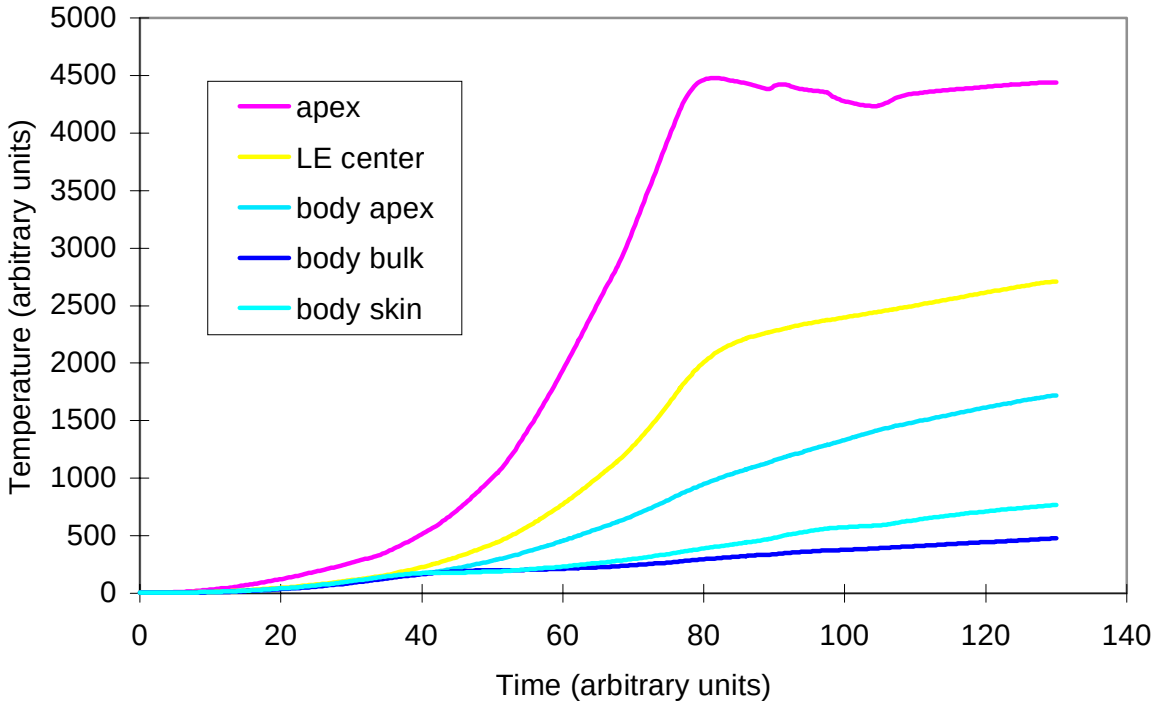


Figure 4. Thermal transient for several points on wing.

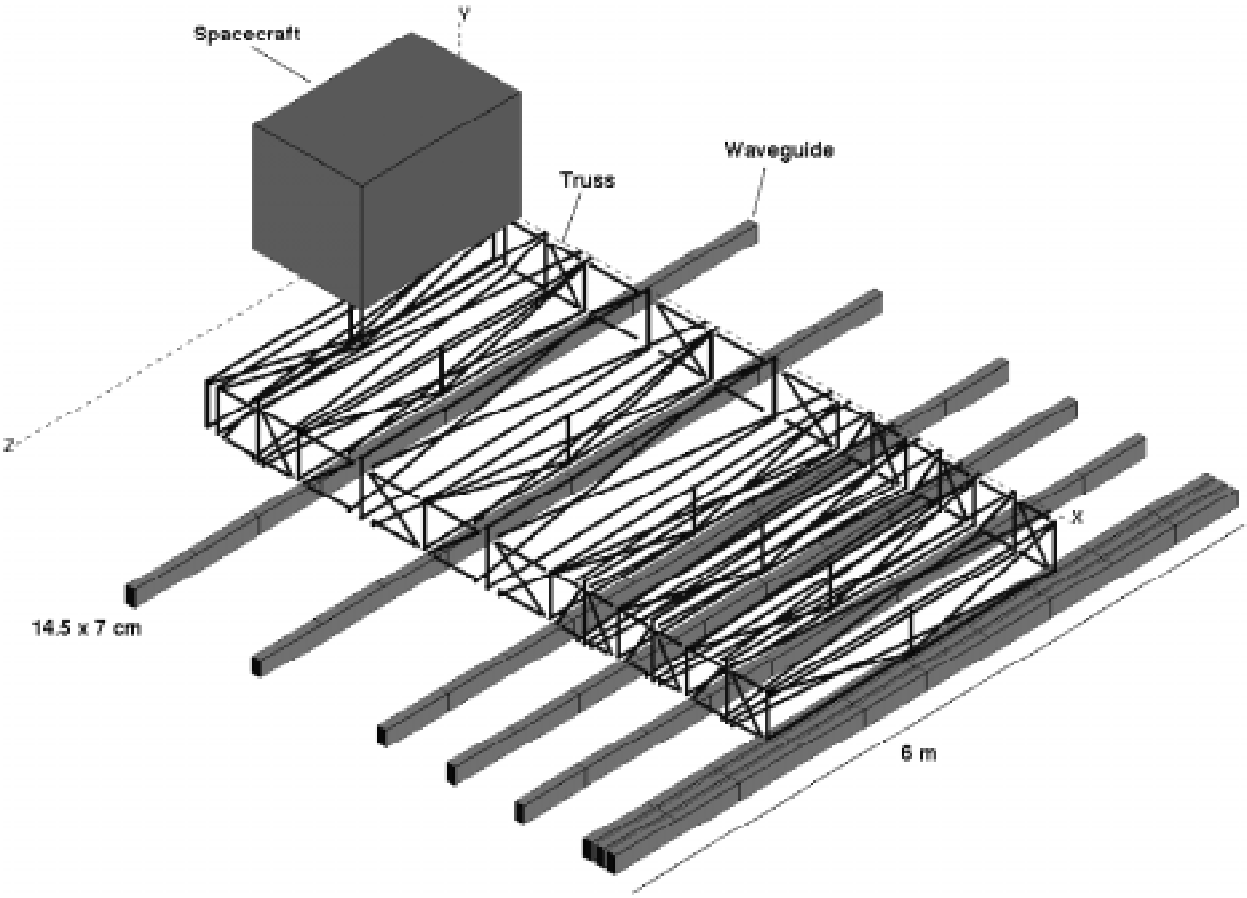


Figure 5. Antenna array geometry in TRASYS model.

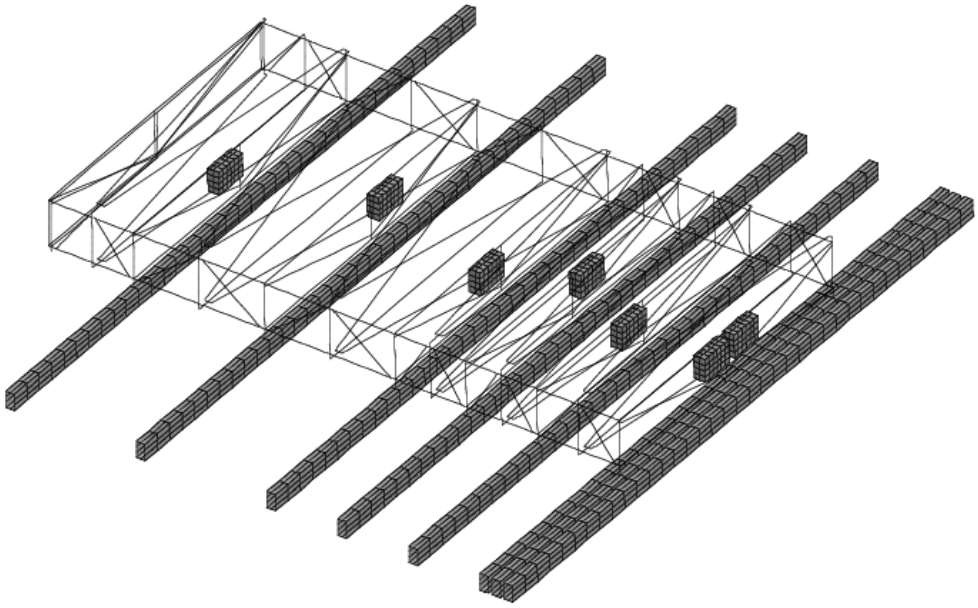

Figure 6. PATRAN model of array.


Figure 7. Predicted thermal distribution for β=60° orbit condition, at single orbit point (in °C).